International Journal of Bridge Engineering (IJBE), Special Issue 2017, pp. 1-24

SEISMIC PERFORMANCE OF HOLLOW-CORE COMPOSITE BRIDGE COLUMNS

Omar I. Abdelkarim[1] and Mohamed A. ElGawady[2]

[1] University of Sherbrooke, Department of Civil Engineering, Canada
[2] Missouri University of Science and Technology, Department of Civil, Architectural & Environmental Engineering, USA
e-mail: abdelkarim.omar@usherbrooke.ca, elgawadym@mst.edu

ABSTRACT: This paper presents the behavior of hollow-core fiber reinforced polymer-concrete-steel (HC-FCS) bridge columns under seismic loading. The HC-FCS column consists of an outer fiber reinforced polymer (FRP) tube, an inner steel tube, and a concrete shell between them. Seven large-scale columns were tested under combined constant axial compressive and cyclic flexural loadings until failure. The investigated columns were one reinforced concrete (RC) column, four HC-FCS columns, and two repaired HC-FCS columns. The outer diameter of each column was 610 mm (24 inches) and the height was 2,413 mm (95 inches) with span-to-depth ratio of 4.0. The steel tube of each HC-FCS column was embedded 635 mm (25 inches) into its own footing while the FRP tube stopped at the top of the footing. The FRP confinement ratio, the steel tube diameter-to-thickness ratio, and the steel tube diameter were examined during this study.

This research revealed that a well-designed HC-FCS column can achieve a high lateral drift of 15.2%. The moment capacity of HC-FCS columns was controlled mainly by the characteristics of the inner steel tube. The maximum lateral drift and displacement ductility were controlled mainly by the ratio of FRP confinement ratio-to- steel tube strength. The plastic hinge length of the HC-FCS columns was controlled by the FRP confinement ratio. The modes of failure of the columns were FRP rupture or steel tube tearing after severe local buckling.

KEYWORDS: Accelerated Bridge Construction; Composites; FRP; Hollow Columns

1 INTRODUCTION

The usage of fiber reinforced polymer (FRP) composites in civil engineering structures continues to grow at an impressive rate due to their low weight-to-strength ratio and high durability under severe conditions [1-14]. Hollow-core FRP-concrete-steel (HC-FCS) column is one of the recent innovation in the

field of bridge construction. This column consists of a concrete shell placed between an outer FRP tube and an inner hollow steel tube [8, 15]. HC-FCS column pieces together the benefits of the FRP, concrete, and steel in one structure. The FRP tube confines the concrete shell hence it increases the concrete ultimate strain. The steel tube provides the column with its flexural and shear strength. The concrete shell laterally supports the steel tube delaying its local buckling. The concrete shell also improves the flexural resistance of the columns. The concrete shell along with the FRP tube, also, protects the steel tube from corrosion effect unlike the exposed steel structures. Hollowing the steel tube reduces the freight costs should the column would be precast which places the HC-FCS column as a viable option for accelerating bridge construction.

Many research groups investigated the behavior of the HC-FCS columns under axial compression loading [e.g., 16-18], flexural loading [e.g., 19, 20], combined flexural and axial compression loading [e.g., 21-24], and vehicle collision [25]. The HC-FCS columns showed high ductile performances under these different loading conditions.

This paper introduces experimental testing of seven large-scale columns under combined axial-flexural loading. The columns were four HC-FCS columns, one RC columns, and two repaired HC-FCS columns. Controlling parameters were investigated in this study including the effects of the FRP confinement ratio, steel tube diameter-to-thickness ratio, and the steel tube diameter. Important terms of the HC-FCS columns including the strength, lateral drift, displacement ductility, failure modes, energy dissipation, and plastic hinge length are discussed as well.

2 EXPERIMENTAL WORK

2.1 Description of specimens

Four virgin and two repaired large-scale cantilever HC-FCS columns were tested under combined constant axial compressive loading and cyclic lateral loading (Table 1, Figs. 1 and 2). One more reinforced concrete (RC) column was tested as a reference specimen. All the tested columns had an outer diameter (D_o) of 610 mm (24 inches) and shear span of 2,413 mm (95 inches) with a shear span-to-depth (H/D_o) ratio of approximately 4.0. The F4-24-RC column had a longitudinal reinforcement of 8φ22 mm (8#7) corresponding to approximately 1.0% of the concrete cross-sectional area and it had a transverse spiral reinforcement of φ13@76 mm (#4 @ 3 inches) corresponding to volumetric reinforcement ratio of approximately 1.0%. The concrete cover beyond the spiral reinforcement was 12.7 mm (0.5 inch). The design and details of construction of the F4-24-RC were selected based on the current construction practice by the Missouri Department of Transportation (MoDOT).

The HC-FCS columns consist of an outer filament wound GFRP tube with thickness of either 3.2 mm (0.125 inch) or 9.5 mm (0.375 inch) (Table 1). The GFRP confinement ratio, calculated using Equation 1, ranged from 0.07 to 0.24.

$$Confinement\ ratio = \frac{2\ f_r\ t_f}{D_o\ f_c'} \quad (1)$$

where f_r is the rupture stress of the GFRP tube in the hoop direction, t_f is the GFRP tube thickness, D_o is the column's outer diameter, and f_c' is the characterized unconfined cylindrical concrete compressive strength.

The steel tube diameter (D_i) was either 406 mm (16 inches) or 356 mm (14 inches) and the thickness (t_s) was either 6.4 mm (0.25 inch) or 12.7 mm (0.5 inch) which presents diameter-to-thickness ratios ranged from 32 to 64 (Table 1).

The FRP tube in the HC-FCS column was truncated at the top face of its footing while the steel tube was embedded into its footing. Similar detail was used at the column head. The typical embedment depth of a steel tube into its footing and its column head was 635 mm (25 inches) representing 1.6D_i to 1.8D_i.

All the HC-FCS columns did not include any shear or flexure rebar. The concrete shell thickness was either 102 mm (4.0 inches) or 127 mm (5.0 inches) representing 16.6% or 20.8% of the column diameter which produces a void ratio of either 44.4% or 34.0% of the column cross-sectional area, respectively.

The expected moment capacity of each column was used to design the footing of each column following the ACI-318 [29] requirements. Each footing had a length, width, and depth of 1,524 mm (60 inches), 1,219 mm (48 inches), and 864 mm (34 inches), respectively.

The footing of the F4-24-RC column had bottom reinforcements of 7 φ 22 mm (7 # 7), top reinforcements of 4 φ 22 mm (4 # 7), and a shear reinforcement of φ13 mm @ 64 mm (#4 @ 2.5 inches; Fig. 1a). The footing of each of columns F4-24-E324, F4-24-P124, and F4-24-E325 had bottom reinforcements of 7 φ 22 mm (7 # 7), top reinforcements of 6 φ 22 mm (6 # 7), and shear reinforcement of φ13 mm @ 64 mm (#4 @ 2.5 inches; Fig. 1b, 1c, and 1e). The footing of column F4-24- E344 had bottom reinforcements of 7 φ 25 (7 # 8), top reinforcements of 6 φ 25 (6 # 8), and a shear reinforcement of φ 13 @ 64 mm (#4 @ 2.5 inches; Fig. 1d).

Table 1. Summary of the Columns' Variables

Column	F4-24-RC	F4-24-E324	F4-24-P124	F4-24-E344	F4-24-E325
Nominal outer diameter (D_o, mm (inch))	610 (24)	610 (24)	610 (24)	610 (24)	610 (24)
Longitudinal reinforcement	8 φ 22 (#8)	N.A.	N.A.	N.A.	N.A.
Transversal reinforcement	spiral φ13-76 mm (#4 - 3 inches)	N.A.	N.A.	N.A.	N.A.
Nominal inner diameter (D_i, mm (inch))	N.A.	406 (16)	406 (16)	406 (16)	356 (14)
Steel tube thickness (t_s, mm (inch))	N.A.	6.4 (0.25)	6.4 (0.25)	12.7 (0.50)	6.4 (0.25)
GFRP Thickness (t_{FRP}, mm (inch))	N.A.	9.5 (0.375)	3.2 (0.125)	9.5 (0.375)	9.5 (0.375)

2.2 Rapid repair technique

Quick repairing of damaged bridge columns after an earthquakes is crucial to allow the search, rescue, and recovery efforts to take place in the affected areas. The target of the quick repair is to partially restore the column's strength and stiffness to permit using the column for a long or short-term as per the engineers' examination recommends [26, 27]. During the course of this study, after testing the virgin columns F4-24-P124 and F4-24-E324 they were quickly repaired and tested as columns F4-24-P124-R and F4-24-E324-R, respectively (Fig. 2).

The repair technique started with removing all big chunks of crushed concrete. Then, a vacuum was used to suck smashed concrete and dust. Three layers of unidirectional GFRP sheets (Tyfo SHE-51) were impregnated with two-component S-epoxy and were wrapped around each column in the bottommost regions where the GFRP tube ruptured. The height of the wrapped regions of the columns F4-24-P124-R and F4-24-E324-R were 1,140 mm (45 inches) and 635 mm (25 inches), respectively (Fig. 3a). This height included the ruptured regions of the GFRP plus an extra height of 127 mm (5 inches).

The wrapping process took approximately 1 hour for each column. Heat chamber using Sonotube paperboard was installed around the wrapped FRP and the temperature was raised up to 50^o C (122^o F) using two heat guns for rapid curing of the GFRP wrapped layers (Fig. 3b). The temperature was measured

and kept constant for 4 hours to ensure the GFRP curing as per the manufacturer recommendations. Grout was injected using low-pressure pumping to replace the damaged concrete chunks (Fig. 3c). Grout injection took about 1 hour for each column. The total time of the rapid repair technique was approximately 6 hours; however, the column was tested 45 hours after starting the repair due to test preparation. Hence, the epoxy cured for 4 hours using high temperature and 41 hours in the laboratory temperature.

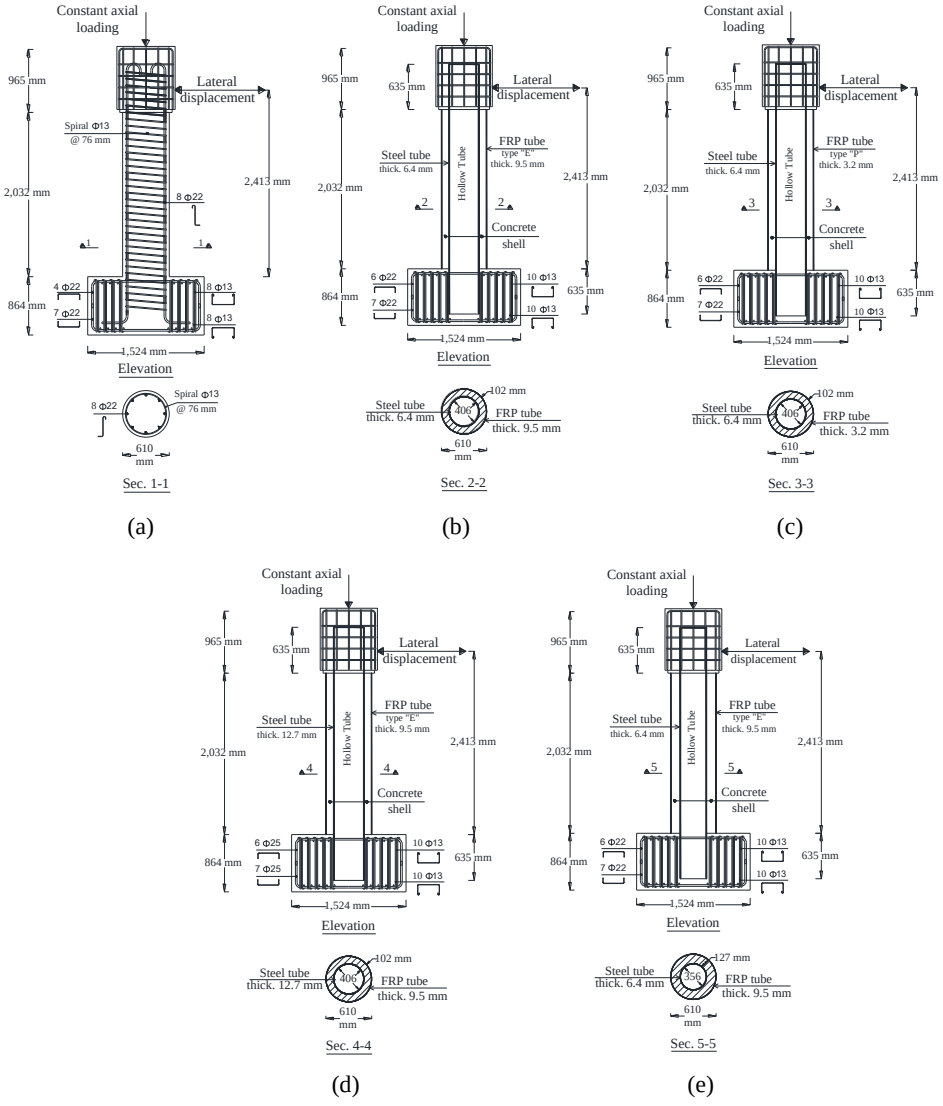

Figure 1. Details of the tested columns: (a) F4-24-RC, (b) F4-24-E324, (c) F4-24-P124, (d) F4-24-E344, and (e) F4-24-345

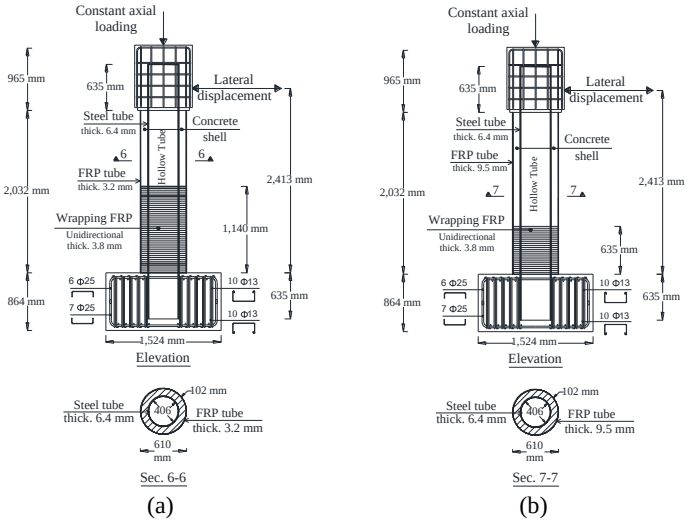

Figure 2. Details of the tested repaired columns: (a) F4-24-P124-R and (b) F4-24-E324-R

2.3 Material properties

The concrete compressive strengths of all the columns at 28 days and at the days of the tests are summarized in Table 2. The properties of the steel and GFRP tubes are summarized in Tables 3 and 4, respectively. The steel tube properties were based on test results of longitudinal coupons prepared according to ASTM A1067 [30]. Two types of GFRP tubes were used on the base of the resin; epoxy and Iso-polyester. This choice was because of the availability in the local market with the different thickness.

Table 2. Concrete strength (f_c') of the investigated columns

Column		F4-24-RC	F4-24-E324	F4-24-P124	F4-24-E344	F4-24-E325
Column f_c', MPa (psi) at	28 days	32.6 (4,725)	32.6 (4,725)	39.8 (5,770)	39.8 (5,770)	35.6 (5,160)
	day of test	36.0 (5,075)	36.0 (5,215)	43.0 (6,235)	53.7 (7,787)	36.8 (5,340)
Footing f_c', MPa (psi) at	28 days	36.6 (5,300)	36.6 (5,300)	56.0 (8,117)	56.0 (8,117)	52.9 (7,670)
	day of test	37.8 (5,480)	38.9 (5,640)	61.4 (8,910)	59.3 (8,605)	56.8 (8,230)

The GFRP tubes properties were based on the manufacturer's data sheets [31,

32]. Longitudinal coupons from each GFRP tube were prepared and tested according to the ASTM D3039 [33] and gave close results to those of the manufacturer. Although, the two GFRP tubes were made of different resins, the hoop FRP rupture strengths were almost the same. The material properties of the GFRP wrapping sheets used in the repair of the columns are summarized in Table 5.

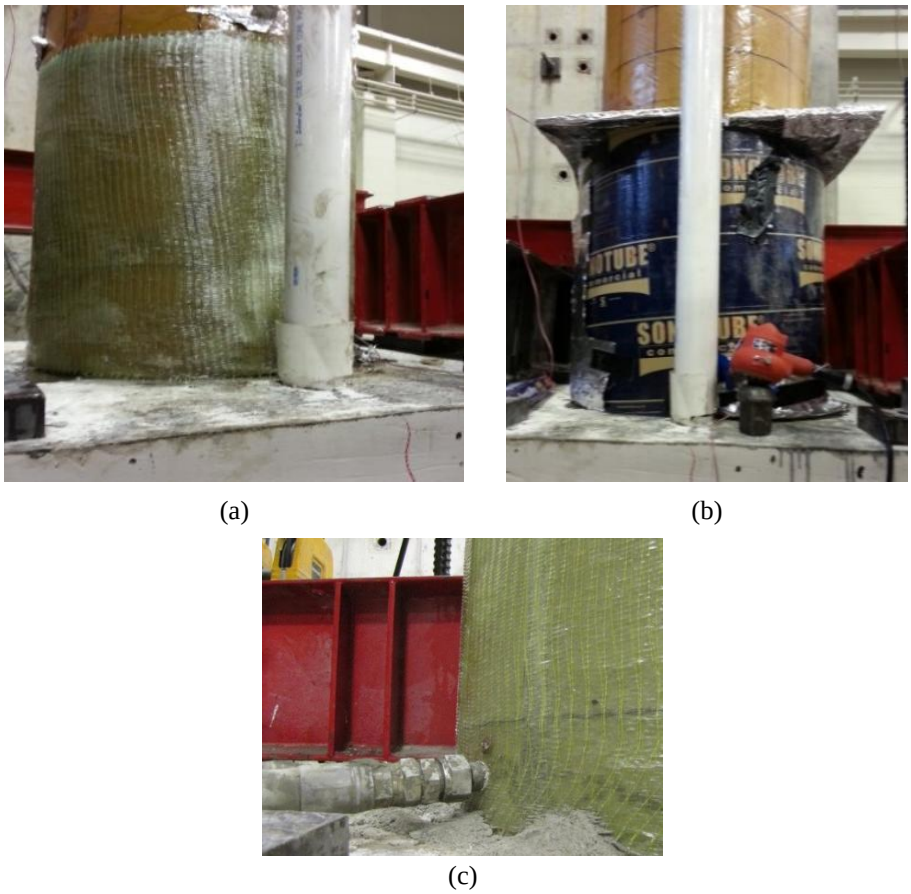

(a) (b)

(c)

Figure 3. Rapid repair technique process: (a) wrapping GFRP layers, (b) applying heat chamber for rapid curing, and (c) injecting grout behind the GFRP tube

Table 3. Steel tube properties based on coupons' tests

Yield stress, MPa (psi)	Ultimate stress, MPa (psi)	Yield strain	Ultimate strain
324 (47,000)	483 (70,000)	0.16%	19.0%

Table 4. FRP Tube Properties based on manufacturer's data (FiberGlass systems [31, 32])

	Axial compression elastic modulus (E_a, GPa (ksi))	Axial ultimate compressive stress (f_{ar}, MPa, (psi))	Axial tension elastic modulus (E_a, GPa (ksi))	Axial ultimate tensile stress (f_{ar}, MPa, (psi))	Hoop elastic modulus (E_h, GPa, (ksi))	Hoop rupture stress (f_{hr}, MPa, (psi))
Epoxy tube (Green Thread HP 16) [31]	4.7 (677)	83.8 (12,510)	11.6 (1,680)	65.7 (9,530)	20.8 (3,020)	276.9 (40,150)
Iso-polyester tube (F-Chem) [32]	9.7 (1,400)	123.4 (17,900)	10.3 (1,500)	64.1 (9,300)	15.2 (2,200)	275.9 (40,000)

Table 5. FRP wrapping Properties based on manufacturer's data (Data from Fyfe Co. LLC. [34])

Total nominal thickness, mm (inch)	Elastic modulus, GPa (ksi)	Tensile strength, MPa (ksi)	Ultimate strain
3.8 (0.15)	26.0 (3,790)	575 (83.4)	2.2%

2.4 Test setup and loading protocol

Each column was subjected to a constant axial compressive loading, using two external prestressed tendons, and cyclic lateral displacement loading (Fig. 4). The tendons were installed at the east and west sides to apply the axial load at the center of the column. The tendons were supported from the top by a rigid beam and from the bottom by the concrete footing. The axial load (P) was kept constant during the test at 490 kN (110 kips) representing 5% of the axial capacity (P_o) of the RC column F4-24-RC. This level of applied load is a common value for the axial loads on bridge columns [35]. The P_o was calculated using Equation 2 [29].

$$P_o = A_s f_y + 0.85\, f_c'(A_c - A_s) \quad (2)$$

where A_s is the cross-sectional area of the longitudinal steel reinforcements, A_c is the cross-sectional area of the concrete column, f_y is the yield stress of the longitudinal steel reinforcements, and f_c' is the characterized unconfined cylindrical concrete compressive strength.

The cyclic lateral displacement loading was applied using two hydraulic actuators connected to the column's loading stub in one end and to the strong wall at the other end (Fig. 4). The lateral loading regime followed FEMA-461 [36] (Fig. 5). The displacement amplitude (a_{i+1}) of the step (i+1) is 1.4 times the proceeding displacement amplitude (a_i) of the step (i) with two executed cycles per each displacement amplitude. Each loading cycle was applied in 100

seconds corresponding to loading rate ranged from 0.25 mm/second (0.01 inch/second) to 1.27 mm/second (0.05 inch/second). The load was applied until failure of the test columns which was defined as when the column lost about 20% of its moment capacity or rupture of the GFRP tube.

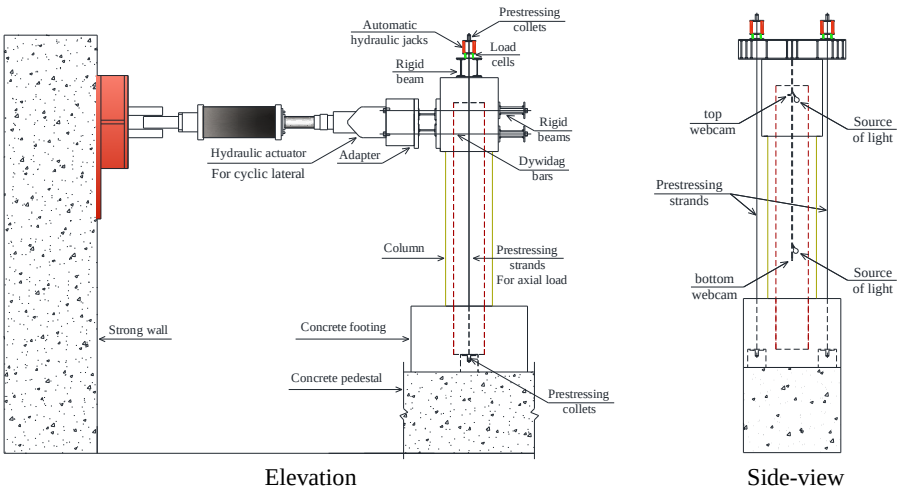

Figure 4. Column test setup

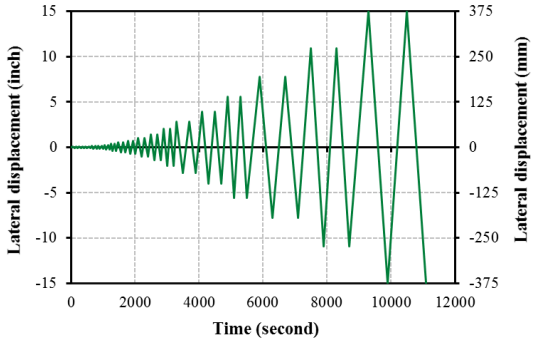

Figure 5. Cyclic lateral displacement loading regime

2.5 Test instrumentations

Linear variable displacement transducers (LVDTs), string potentiometers (SPs), and strain gauges were used to measure the global and local deformations of the tested columns (Fig. 6). Four vertical LVDTs were used at each north and south faces of the column to measure the vertical displacement at four cross-section levels to determine the column's curvature at each level. However, each footing was fixed to the strong floor by dywidag bars and steel beams, a horizontal and vertical LVDTs were attached to each footing to measure if there was any

sliding or uplifting. For the HC-FCS columns, four vertical and four horizontal strain gauges (SGs) were attached inside each steel tube at north, west, south, and east directions at 9 levels with 127 mm (5 inches) intervals with total SGs of 72. Four vertical and four horizontal strain gauges (SGs) were attached on each GFRP tube at north, west, south, and east directions at 6 levels with 127 mm (5 inches) intervals with total SGs of 48. Total of fourteen electrical strain gauges (SGs) were symmetrically installed, on the two north and south longitudinal steel rebars of the column F4-24-RC at seven levels, at the top of footing level and 3 above and below that level, with 101.6 mm (4 inches) intervals. Two webcams were installed inside the steel tube of the F4-24-P124 column to monitor the deformations of the steel tube (Fig. 4).

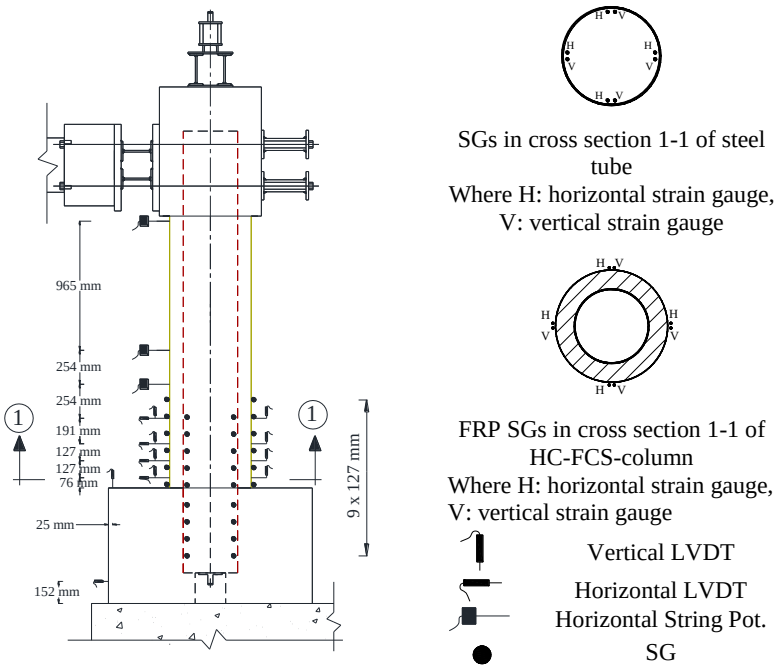

Figure 6. Layout of the instrumentations (1 mm = 0.04 inch)

3 RESULTS AND DISCUSSIONS

Figure 7 illustrates the hysteretic lateral drift vs. moment of the seven investigated columns. The lateral drift of each column was obtained by dividing the lateral displacement measured from the actuators and corrected for any footing sliding or uplifting, by the column's height of 2,413 mm (95 inches). All the footing displayed negligible values of sliding and uplifting. The moment at the base of each column was obtained by multiplying the force collected from the actuators' loading cells by the column's height of 2,413 mm (95 inches).

3.1 Column F4-24-RC

As shown in the Fig. 7a, the column F4-24-RC behaved linearly up to a lateral drift of 0.5% followed by yielding of the flexural rebar at drift of 1.1% and gradual stiffness degradation up to a lateral drift of 2.0%. The average moment capacity of the column was 594 kN.m (438 kip.ft) which occurred at a lateral drift of approximately 5.1%. The failure of the column occurred at the first cycle of the lateral drift of 10.9% due to fracture of one rebar at each of the north and south sides of the column. During the second cycle of the same drift, other two rebars fractured at each of the north and south sides with a total of six rebars fractured out of eight rebars (Fig. 8a). The severe damage zone of the column was within the bottommost 229 mm (9 inches) of the column. The readings of the strain gauge showed that the maximum axial tensile strain of the farthest flexural steel rebars was 18,000 με. The farthest steel rebars buckled in compression at a lateral drift of 7.5%. By the end of the test, the column displayed a displacement ductility of 9.9.

3.2 Columns F4-24-E324 and F4-24-P124

Both columns were identical but the GFRP thickness and resins. Both columns behaved linearly up to a lateral drift of 0.9% followed by yielding of the steel tube in tension at a lateral drift of 1.0% and 1.3% in the case of F4-24-E324 and of F4-24-P124, respectively. Both columns displayed gradual stiffness degradation up to a lateral drift of 2.8% and 2.6% in the case of F4-24-E324 and of F4-24-P124, respectively (Figs. 7b and 7c). Both columns reached approximately to the same average moment capacity being 732 kN.m (540 kip.ft) and 748 kN.m (552 kip.ft) which occurred at a lateral drift of 2.8% and 2.6% in the case of F4-24-E324 and of F4-24-P124, respectively. However, beyond the peak moment capacity the columns behaved differently.

In the case of F4-24-E324, the moment was almost constant up to a lateral drift of approximately 6.0%. After that, the moment reduced gradually until failure occurred at a lateral drift of 15.2% when the GFRP tube ruptured at an ultimate hoop strain of 13,130 με (Fig. 8b).

In the case of F4-24-P124, the column suffered stiffness softening until the failure of the column at a lateral drift of 5.8% when the GFRP tube ruptured at an ultimate hoop strain of 6,150 με (Fig. 8c). The strain readings showed that the maximum axial tensile strains of the steel tubes were 11,000 με and 14,000 με in the case of F4-24-E324 and of F4-24-P124, respectively. Furthermore, the steel tube locally buckled at a lateral drift of 3.0% in the case of F4-24-E324 while it did not buckle in the case of F4-24-P124 due to the low confinement ratio. The steel tube local buckling of the F4-24-E324 was the reason of the lower axial tensile strain than that of the F4-24-P124 as the steel tube could not gain more strains with cycling the column. The no buckling behavior was confirmed through axial strain measurement as well as the video cameras

inserted inside the steel tube. The investigation after the test completion showed that the concrete shell within the bottommost 152 mm (6 inches) of the F4-24-E324 was powder indicating good confinement from the GFRP and steel tubes. The concrete shell of the F4-24-P124 displayed moderate cracking but not reach to the same conditions of that of the F4-24-E324 due to the low confinement ratio. The difference in the confinement ratio also affected the displacement ductility. The columns displayed displacement ductility of 15.2, and 4.5 in the case of F4-24-E324 and of F4-24-P124, respectively.

3.3 Column F4-24-E344

The column F4-24-E344 behaved linearly up to a lateral drift of 0.5% followed by the appearance of a fine vertical crack at the midway of the footing length at a lateral drift of 1.4%. Further cycling led to yielding of the steel tube in tension at a lateral drift of 1.8% and propagation of cracks into the footing shaping the common cone-shape of the pullout failure due to the insufficient steel tube embedment length. Gradual stiffness degradation initiated at 0.5% and continued up to a lateral drift of 7.7% (Fig. 7d). The hysteretic curve of the column displayed significant pinching during the reloading cycles (Fig. 7d). The average moment capacity of the column was 1,186 kN.m (875 kip.ft) which occurred at a lateral drift of 7.7%. Severe damage of the footing occurred at a lateral drift of 8.0% and continued until the test was ended at a drift of 11.6% when the column strength dropped by 15% (Fig. 8d). The maximum hoop tensile strain of the GFRP tube was 11,800 με. The maximum axial tensile strain of the steel tube was 15,200 με while no steel tube buckling was recorded. The column displayed a displacement ductility of 6.4.

3.4 Column F4-24-E325

The column F4-24-E345 behaved linearly up to a lateral drift of 0.4% followed by tensile yielding of the steel tube at a lateral drift of 1.9% and gradual stiffness degradation up to a lateral drift of 3.0% when the column reached its moment strength of 677 kN.m (499 kip.ft) (Fig. 7e). Beyond drift 3%, the moment gradually decreased until a drift of 11.4% when the column strength dropped by 20% of the moment capacity which was considered as the failure of the column.

However, cycling the column continued until a lateral drift of 15.6% when the actuators reached its maximum stroke. No damage occurred to the GFRP tube by the end of the test with the maximum recoded hoop tensile strain of 10,000 με. The maximum axial tensile strain of the steel tube was 10,600 με while the steel tube locally buckled at a lateral drift of 3.2%. Once the test was concluded, the steel tube was exposed and investigated by removing part of the GFRP tube. It was found that the steel tube suffered severe local buckling along with steel rupture within the bottommost 127 mm (5 inches) of the column (Fig.

8e). The column displayed a displacement ductility of 6.0.

3.5 Columns F4-24-E325 versus F4-24-RC

The columns F4-24-E325 and F4-24-RC had approximately an equivalent steel weight of 113 kg per column in the form of steel tube or rebars and spiral reinforcement, respectively. As shown in Fig. 9, both columns displayed similar behavior up to lateral drift of 10.9% when the column F4-24-RC failed while column F4-24-E325 failed at drift of 15.2%. Both columns ultimately displayed steel fracture. The column F4-24-E325 could achieve a higher moment capacity than that of the column F4-24-RC by approximately 14%. The residual flexural strength of the column F4-24-E325 at a lateral of 15.6% was 311 kN.m (230 kip.ft) representing 46% of its moment capacity. The residual flexural strength of the column F4-24-RC at a lateral of 10.9% was 196.5 kN.m (145 kip.ft) representing 33% of its moment capacity. In addition, the construction of the F4-24-E325 column with the construction details of the HC-FCS columns took approximately 10% of the time required in constructing the column F4-24-RC at the High-bay Structures Lab at the Missouri University of Science and Technology.

3.6 Columns F4-24-P124-R versus F4-24-P124

The F4-24-P124-R was the repaired column of the F4-24-P124 using GFRP wrapping. Figure 7f illustrates the hysteretic lateral drift-moment relation of the column F4-24-P124-R. Figure 10 illustrates the hysteretic lateral drift-moment relation of the column F4-24-P124-R versus that of the column F4-24-P124. As shown in both figures the repaired column displayed higher deformation capacity due to the higher confinement ratio of the repair, i.e., the column F4-24-P124 and F4-24-P124-R had confinement ratios of 0.07 and 0.17, respectively. The confinement ratio of the repaired column was approximately 71% of that used for column F4-24-E324 who displayed deformation capacity of 15.2%.

The average moment capacity of the column F4-24-P124-R was 693 kN.m (512 kip.ft) at a lateral drift of 8.0% while the average moment capacity of the virgin column F4-24-P124 was 748 kN.m (552 kip.ft) at a lateral drift of 2.6%. The column F4-24-P124-R failed by rupture of GFRP wrapping layers at a lateral drift of 13.2% (Fig. 8f). Figure 10 showed that the repaired column F4-24-P124-R could successfully retrieve 95% of the moment capacity and 61% of the initial stiffness of the virgin column. This reduction in the initial stiffness of the repair column is attributed to the residual strains in the steel tube before the repair process. However, such residual strains did not affect the moment capacity of the column F4-24-P124-R.

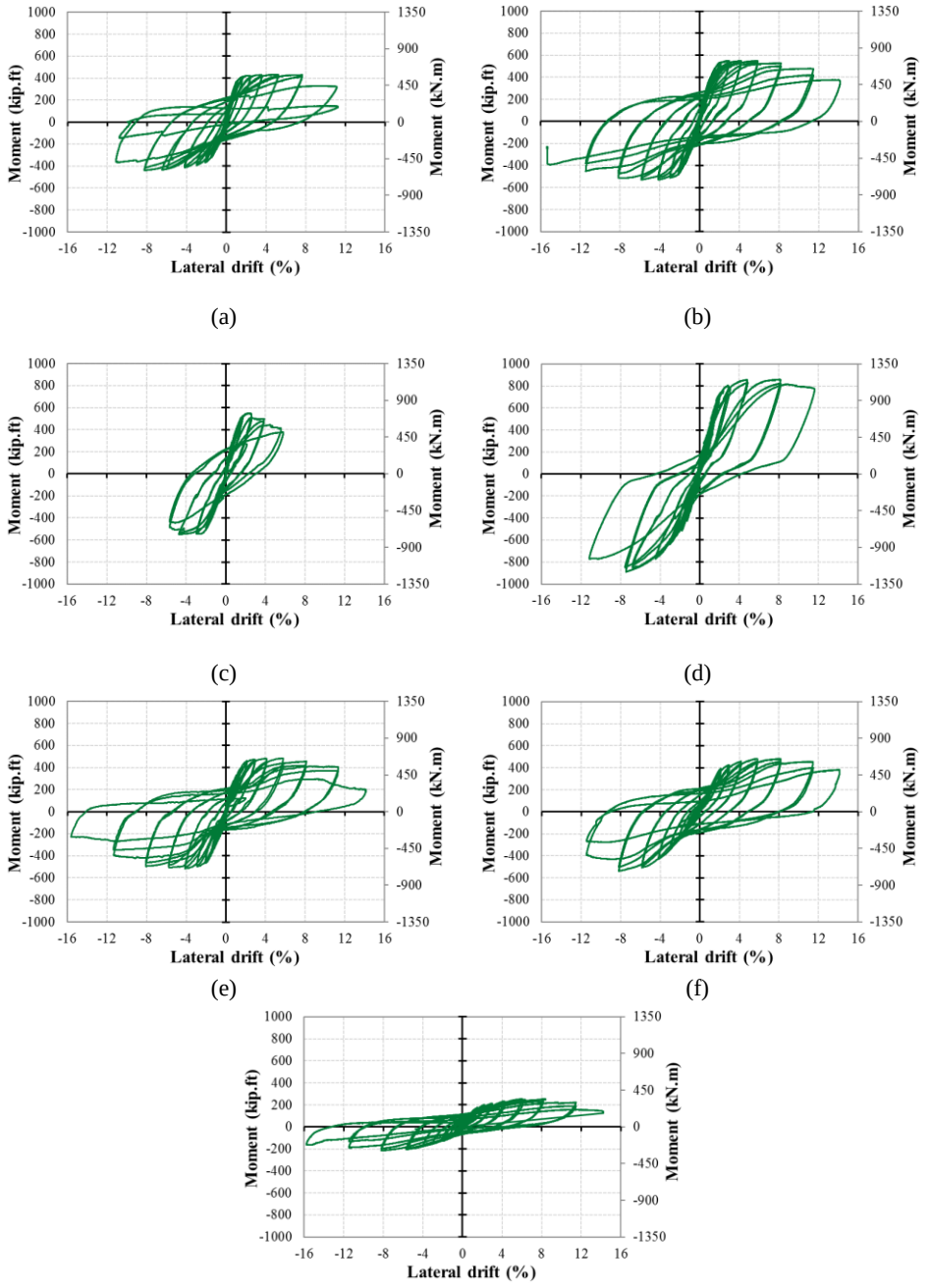

Figure 7. Lateral drift-moment relation of the columns: (a) F4-24-RC, (b) F4-24-E324, (c) F4-24-P124, (d) F4-24-E344, (e) F4-24-E325, (f) F4-24-P124-R, and (g) F4-24-E324-R

F4-24-RC: rebar fracture

F4-24-E324: rupture of FRP tube

F4-24-P124: rupture of FRP tube

F4-24-E344: footing cone failure

F4-24-E325: steel tube tearing

F4-24-P124-R: rupture of FRP wrapped layers

F4-24-E324-R: steel tube tearing

Figure 8. Failure modes of the investigated columns

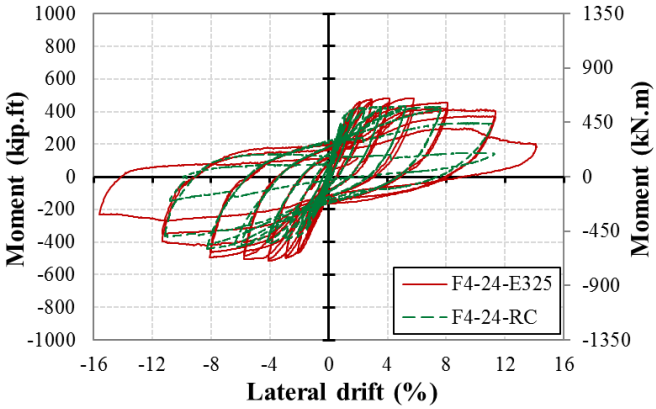

Figure 9. Lateral drift-moment relation of the columns F4-24-RC and the F4-24-E325

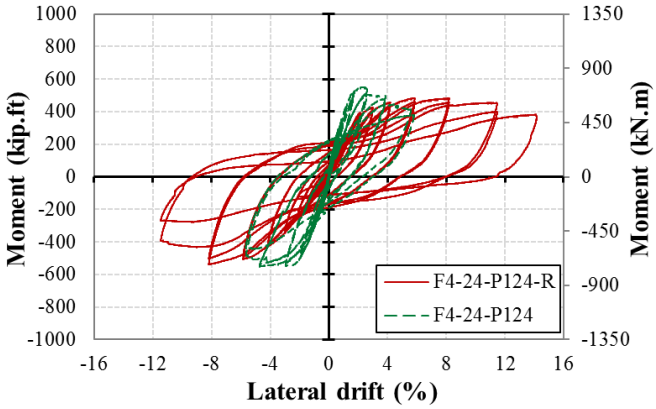

Figure 10. Lateral drift-moment relation of the columns F4-24-P124-R and F4-24-P124

3.7 Columns F4-24-E324-R versus F4-24-E324

The F4-24-E324-R was the repaired column of the F4-24-E324 using GFRP wrapping. Figure 7g illustrates the hysteretic lateral drift-moment relation of the column F4-24-E324-R. Figure 11 illustrates the hysteretic lateral drift-moment relation of the column F4-24-E324-R versus that of the column F4-24-E324. The average moment capacity of the column F4-24-E324-R was 318 kN.m (235 kip.ft) at a lateral drift of 6.0% while the average moment capacity of the virgin column F4-24-E324 was 732 kN.m (540 kip.ft) at a lateral drift of 2.8%. The column F4-24-E324-R failed by the steel tube tearing due to the low cyclic fatigue (Fig. 8g). Figure 11 showed that the repaired column neither able to retrieve the strength nor the stiffness of the virgin column F4-24-E324 as the steel tube of the virgin column suffered severe inelastic local buckling along with reaching to a very high lateral drift of 15.2% before the GFRP tube ruptured. This behavior indicated that when an HC-FCS column suffers high

damage during an earthquake it cannot be repaired using the proposed simple technique and further measures need to be taken.

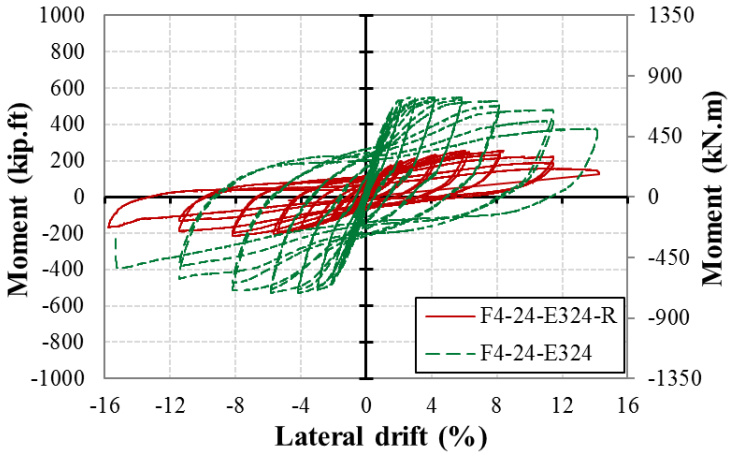

Figure 11. Lateral drift-moment relation of the columns F4-24-E324-R and F4-24-E324

3.8 FRP confinement and steel tube strength effects

This section discusses the effects of the FRP confinement, the thickness, and diameter of the steel tube on design parameters of the virgin HC-FCS columns.

3.8.1 Moment capacity

The moment capacity of a HC-FCS column was mainly controlled by the steel tube properties and dimensions. Columns F4-24-E324 and F4-24-P124 had similar steel tube; however, the FRP tube thickness of the column F4-24-E324 was 3 times that of the column F4-24-P124. Both columns displayed the same moment capacity. Figure 12 and Equations 3 to 5 illustrate the relation between the steel tube strength ($ST_s = D_i t_s F_u$) and the moment capacity of the investigated columns. The equations were developed based on simplification of the regression analyses results. The moment capacity increased linearly with increasing the steel tube strength. However, few columns investigated during this study and it is anticipated that there is a threshold of steel tube strength beyond which the relationship will be nonlinear due to the change in the mode of failure. Furthermore, the investigated columns were subjected to low level of axial load which is common in a bridge column. Therefore, the contribution of the axial load did not appear in the Equations.

$$M_c = 6.0\ (ST_s)^{0.68} \quad \text{SI units} \quad (3)$$

$$M_c = 12.0\ (ST_s)^{0.68} \quad \text{Custom units} \quad (4)$$

$$ST_s = D_i t_s F_u \quad (5)$$

Where M_c is the moment capacity in kN.m (kip.ft.), ST_s is the steel tube strength, D_i is the steel tube outer diameter in mm (inch), t_s is the steel tube thickness in mm (inch), and F_u is the ultimate stress of the steel tube in GPa (ksi).

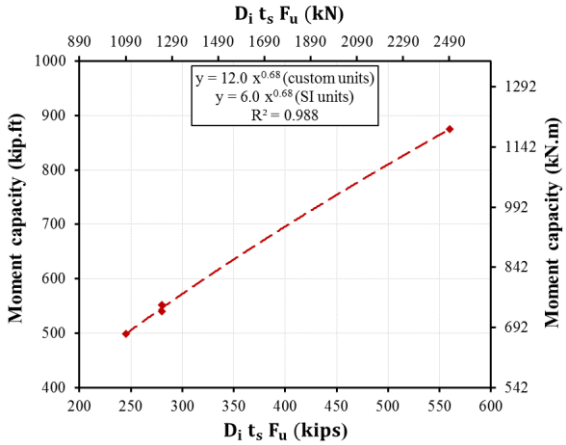

Figure 12. Steel tube strength versus the moment capacity of the HC-FCS columns

3.8.2 Maximum lateral drift and displacement ductility

The relation between the FRP confinement ratio (*CR*) and the steel tube strength (ST_s) is very important for understanding the behavior of the HC-FCS columns. There is an interaction between the confinement ratio, steel tube strength, and lateral pressure due to concrete dilation under compressive stresses. When the *CR* increases with constant ST_s, the concrete lateral pressure increases on the inner steel tube and vise versa. The maximum lateral drift and displacement ductility of the HC-FCS column are controlled by the ratio between the *CR* and ST_s. Figure 13a and Equations 6 and 7 illustrate the relation between the CR/ST_s ratio and the maximum lateral drift. Regression analysis showed that the best fit for the available data is a second-degree equation with R^2 values of 0.909 and 0.936 in the case of drift and displacement ductility, respectively. The equations were developed based on simplification of the regression analyses results. More data is required to improve the proposed relationships. Based on the available date, the peak drift, 21%, occurred at CR/ST_s ratio of $1.42 \times 10^{-4}\ \frac{1}{kN}$ ($6.3 \times 10^{-4}\ \frac{1}{kip}$). When the CR/ST_s ratio is higher than $1.42 \times 10^{-4}\ \frac{1}{kN}$ ($6.3 \times 10^{-4}\ \frac{1}{kip}$), the FRP tube stiffness is high enough compared to that of the inner steel tube and hence the concrete dilation demand is much higher on the inner steel tube. In this case, the steel tube is subjected to very high demand and displays severe local buckling similar to columns F4-24-E324 and F4-24-E325.

Furthermore, when the CR/ST_s ratio is lower than $1.42 \times 10^{-4}\ \frac{1}{kN}$ ($6.3 \times 10^{-4}\ \frac{1}{kip}$), the FRP tube is subjected to more lateral pressure demand due to concrete dilation. In this case, the steel tube does not suffer much damage similar to columns F4-24-E344 and F4-24-P124 where their steel tubes did not suffer any local buckling.

Figure 13b and Equations 8 and 9 illustrate the relation between the CR/ST_s ratio and the displacement ductility. The peak displacement ductility of 21.5 was found at CR/ST_s ratio of $1.39 \times 10^{-4}\ \frac{1}{kN}$ ($6.2 \times 10^{-4}\ \frac{1}{kip}$). The relation between the CR/ST_s ratio and the displacement ductility was very similar to the relation between the CR/ST_s ratio and the maximum lateral drift.

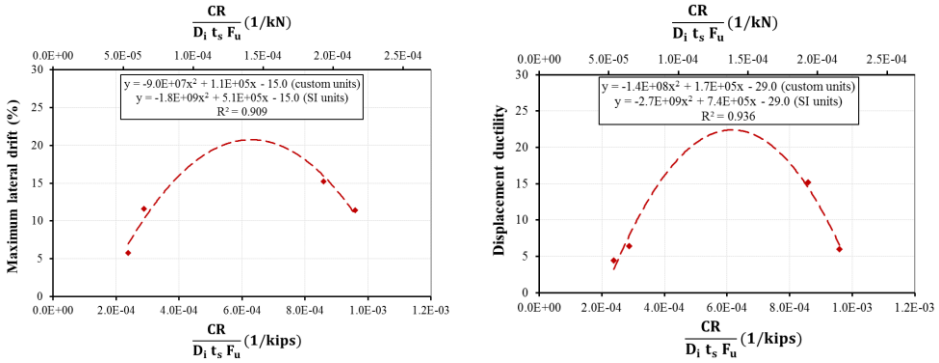

Figure 13. Confinement ratio/steel tube strength versus: (a) the maximum lateral drift and (b) the displacement ductility

$$\delta_m = -1.8E9\ (\frac{CR}{ST_s})^2 + 5.1E5\ \left(\frac{CR}{ST_s}\right) - 15.0 \qquad \text{- SI units} \qquad (6)$$

$$\delta_m = -9.0E7\ (\frac{CR}{ST_s})^2 + 1.1E5\ \left(\frac{CR}{ST_s}\right) - 15.0 \qquad \text{- Custom units} \qquad (7)$$

Where δ_m is the maximum lateral drift, ST_s is the steel tube strength in $\frac{1}{kip}$ for custom units and $\frac{1}{kN}$ for SI units, $5.2 \times 10^{-5}\ \frac{1}{kN}$ ($2.3 \times 10^{-4}\ \frac{1}{kip}$) $< \frac{CR}{ST_s} < 2.2 \times 10^{-4}\ \frac{1}{kN}$ ($9.6 \times 10^{-4}\ \frac{1}{kip}$)

$$\mu = -2.7E9\ (\frac{CR}{ST_s})^2 + 7.4E5\ \left(\frac{CR}{ST_s}\right) - 29.0 \qquad \text{- SI units} \qquad (8)$$

$$\mu = -1.4E8\ (\frac{CR}{ST_s})^2 + 1.7E5\ \left(\frac{CR}{ST_s}\right) - 29.0 \qquad \text{- Custom units} \qquad (9)$$

Where μ is the displacement ductility, ST_s is the steel tube strength in $\frac{1}{kip}$ for custom units and $\frac{1}{kN}$ for SI units, $5.2 \times 10^{-5} \frac{1}{kN}$ $(2.3 \times 10^{-4} \frac{1}{kip})$ $< \frac{CR}{ST_s} <$ 2.2 $\times 10^{-4} \frac{1}{kN}$ $(9.6 \times 10^{-4} \frac{1}{kip})$

3.8.3 Energy dissipation

The energy dissipation (*ED*) of each column was calculated as the summation of the energy dissipation of the first cycle for each drift. The energy dissipation at each drift was determined as the enclosed area of the hysteretic loop of the force-displacement relation. The *EDs* of the columns F4-24-E324, F4-24-P124, F4-24-E344, and F4-24-E325 were 452 kN.m (333 kip.ft), 98 kN.m (72 kip.ft), 302 kN.m (223 kip.ft), and 460 kN.m (340 kip.ft), respectively. Figure 14 and Equations 10 and 11 illustrate the relation between the CR/ST_s ratio and the *ED* of the investigated columns. simplification of the regression analyses results. The peak *ED* of 533 kN.m (395 kip.ft) was found at CR/ST_s ratio of 1.62 $\times 10^{-4} \frac{1}{kN}$ $(7.2 \times 10^{-4} \frac{1}{kip})$.

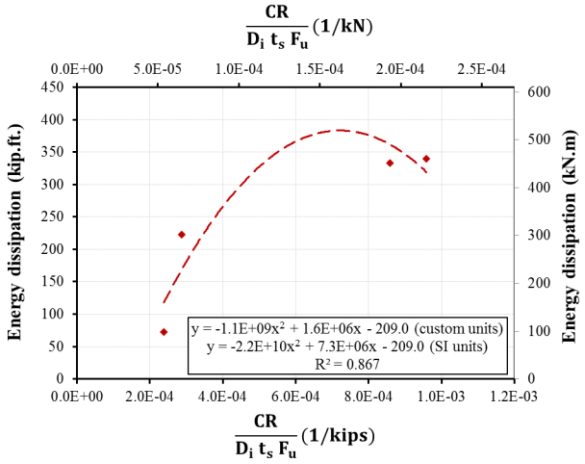

Figure 14. Confinement ratio/steel tube strength versus the energy dissipation of the HC-FCS columns

$$ED = -2.2E10\,(\frac{CR}{ST_s})^2 + 7.3E6\,\left(\frac{CR}{ST_s}\right) - 209.0 \qquad \text{- SI units} \qquad (10)$$

$$ED = -1.1E9\,(\frac{CR}{ST_s})^2 + 1.6E6\,\left(\frac{CR}{ST_s}\right) - 209.0 \qquad \text{- Custom units} \qquad (11)$$

Where ED is the total energy dissipated after cycling the column in kip.ft for custom units and in kN.m for SI units, ST_s is the steel tube strength in $\frac{1}{kip}$ for

custom units and $\frac{1}{kN}$ for SI units, $5.2 \times 10^{-5} \frac{1}{kN}$ ($2.3 \times 10^{-4} \frac{1}{kip}$) < $\frac{CR}{ST_s}$ < $2.2 \times 10^{-4} \frac{1}{kN}$ ($9.6 \times 10^{-4} \frac{1}{kip}$)

3.8.4 Plastic hinge length

The region where concentrated nonlinear deformations take place in a structural element is defined as the plastic hinge length (l_p). In the case of conventional reinforced concrete columns l_p includes two regions, i.e., the steel yield penetration depth into the footing region (l_{py}) and the region above the footing where the nonlinear deformations take place (l_a). In the case of the HC-FCS columns, the l_a was linked to the FRP tube hoop strains and defined as the region from the top of footing to where the FRP hoop strain dropped to one-third of its maximum value at the same drift cycle [37]. Using this definition, the l_a of the columns F4-24-E324, F4-24-P124, F4-24-E344, and F4-24-E325 was 10.3%, 8.9%, 4.7%, and 8.9% of the columns' shear span (H), respectively. These results agreed with the damaged lengths of these columns that was noticed in the investigation after the tests along with the curvature results measured by the LVDTs. Per the previous definition of the l_a, the FRP confinement ratio is the main parameter affecting the l_a of the HC-FCS columns. Figure 15 and Equation 12 illustrate the nonlinear relation between the confinement ratio and the l_a/H of the investigated columns. The equations were developed based on simplification of the regression analyses results. The lowest value of the l_a/H was 4.6% which happened at a confinement ratio of 0.15.

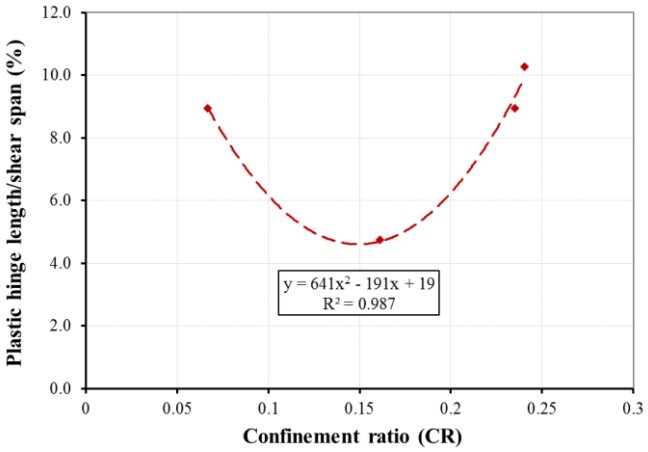

Figure 15. FRP confinement ratio versus the percentage of plastic hinge/shear span of the HC-FCS columns

$$L_a/H = 641\,CR^2 - 191\,CR + 19 \quad (12)$$

Where L_a is the plastic hinge length above the footing level, H is the column shear span, and CR is the FRP tube confinement ratio calculated using Equation (2), $0.07 < CR < 0.24$

4 CONCLUSIONS

This paper presents a comprehensive study on the behavior of hollow-core fiber reinforced polymer-concrete-steel (HC-FCS) bridge columns. The study included testing seven large-scale columns under combined constant axial compressive and cyclic flexural loadings until failure. The columns were: one reinforced concrete (RC) column, four HC-FCS columns, and two repaired HC-FCS columns. Each HC-FCS column consisted of an outer fiber reinforced polymer (FRP) tube, an inner hollow steel tube, and a concrete shell between them. The outer diameter of each column was 610 mm (24 inches) and the height was 2,413 mm (95 inches) with span-to-depth ratio of 4.0. The steel tube of each HC-FCS column was embedded into the footing by 635 mm (25 inches) while the FRP tube stopped at the top of footing. The FRP tube confinement ratio, the steel tube diameter, and the steel tube thickness were changed to investigate their effects on the behavior of the HC-FCS columns. The study revealed the following:

- The HC-FCS columns present superior performance compared to well-designed reinforced concrete columns.
- The HC-FCS achieved a high lateral drift of 15.2%.
- Moderately damaged HC-FCS column was effectively and quickly repaired using FRP wrapping.
- Regression analyses showed that the peak maximum lateral drift, displacement ductility, and energy dissipation could be achieved when the ratio of the FRP confinement ratio/steel tube strength was between $1.39 \times 10^{-4} \frac{1}{kN}$ ($6.2 \times 10^{-4} \frac{1}{kip}$) and $1.62 \times 10^{-4} \frac{1}{kN}$ ($7.2 \times 10^{-4} \frac{1}{kip}$). However, more data is still required to confirm this conclusion.
- Regression analyses showed that the FRP confinement ratio of 0.15 would give the lowest plastic hinge length. However, more data is still required to confirm this conclusion.

ACKNOWLEDGMENTS

This research was supported by the Missouri Department of Transportation (MoDOT) and Mid-American Transportation Center (MATC). In kind contribution from ATLAS Tube is appreciated. Discounts on FRP tubes from Grace Composites and FRP Bridge Drain Pipe are also appreciated. The authors also extend their appreciation to the National University Transportation Center (NUTC) at the Missouri University of Science and Technology (Missouri S&T). The authors appreciate the help from graduate students Sujith Anumolu, Ahmed

Gheni, Mohanad Abdulazeez, and Song Wang during running the experimental work described in this manuscript. Appreciation is also extended to the laboratory staff Brian Swift, Gary Abbott, and John Bullock. Also, the feedback and discussion with MoDOT engineers Gregory Sanders and William Stone, MoDOT is highly appreciated. However, any opinions, findings, conclusions, and recommendations presented in this paper are those of the authors and do not necessarily reflect the views of the sponsors.

REFERENCES

[1] Youssf, O., ElGawady, M. A., Mills, J. E., Ma, X., 2014. "Finite element modelling and dilation of FRP-confined concrete columns" Engineering Structures, 79 (15), 70-85.
[2] Youssf, O., ElGawady, M. A., Mills, J., 2016. "Static cyclic behaviour of FRP-confined crumb rubber concrete columns" Engineering Structures, Vol. 113, 371–387
[3] Tuwair, H., Hopkins, M., Volz, J., ElGawady, M. A., Mohaned, M., Chandrashekhara, K., Birman, V., 2015. "Evaluation of sandwich panels with various polyurethane foam-cores and ribs" J. Composites: Part B, 79, 262-276.
[4] Fam, A., Flisak, B., Rizkalla, S. (2003). "Experimental and analytical modeling of concrete-filled fiber-reinforced polymer tubes subjected to combined bending and axial loads." ACI Structural Journal, 100 (4), pp. 499-509.
[5] Shao, Y. and Mirmiran, A. (2005). "Experimental Investigation of Cyclic Behavior of Concrete-Filled Fiber Reinforced Polymer Tubes." J. Compos. Constr., 9(3), 263–273.
[6] Benmokrane, B., El-Salakawy, E., El-Ragaby, A., and Lackey, T. (2006). "Designing and testing of concrete bridge decks reinforced with glass FRP bars." Journal of Bridge Engineering, 11(2): 217–229.
[7] Zhu, Z., Ahmad, I., and Mirmiran, A. (2006). "Seismic performance of concrete-filled FRP tube columns for bridge substructure." J. Bridge Eng., 11(3), 359–370.
[8] Shakir-Khalil, H., and Illouli, S. (1987). "Composite columns of concentric steel tubes." Proc., Conf. on the Design and Construction of Non-Conventional Structures, Vol. 1, London, pp. 73–82.
[9] ElGawady, M. and Dawood, H. (2012). "Analysis of segmental piers consisted of concrete filled FRP tubes." Engineering Structures, Vol. 38, pp. 142-152.
[10] ElGawady, M. and Sha'lan, A. (2011). "Seismic Behavior of Self-Centering Precast Segmental Bridge Bents." J. Bridge Eng., 16(3), 328–339.
[11] ElGawady, M., Booker, A., and Dawood, H. (2010). "Seismic Behavior of Posttensioned Concrete-Filled Fiber Tubes." J. Compos. Constr., 14(5), 616–628.
[12] Moon, J., Lehman, D. E., Roeder, C. W., and Lee, H. E. (2013). "Strength of Circular Concrete-Filled Tubes with and without Internal Reinforcement under Combined Loading." Journal of Structural Engineering, 139(12).
[13] Qasrawi, Y., Heffernan, P. J., & Fam, A. (2014). "Performance of Concrete-Filled FRP Tubes under Field Close-in Blast Loading." J. Compos. Constr., 10.1061/(ASCE)CC.1943-5614.0000502 , 04014067.
[14] Youssef, O; ElGawady, M. A., ills, J. (2015). "Displacement and plastic hinge length of FRP-confined circular reinforced concrete columns" Engineering Structures, Vol. 10, 465 – 476.
[15] Teng, J.G., Yu, T., and Wong, Y.L. (2004). "Behavior of Hybrid FRP-Concrete-Steel Double-Skin Tubular Columns." Proc. 2nd Int. Conf. on FRP Composites in Civil Engineering, Adelaide, Australia, 811-818.
[16] Abdelkarim, O. I. and ElGawady. M. A. (2016b) "Behavior of hollow FRP–concrete–steel columns under static cyclic axial compressive loading." Engineering Structures 123: 77-88.
[17] Yu, T., Teng, J. G., and Wong, Y. L. (2010). "Stress-Strain Behavior of Concrete in Hybrid

FRP-Concrete-Steel Double-Skin Tubular Columns." Journal of Structural Engineering, 10.1061/(ASCE)ST.1943-541X.0000121, 379-389.
[18] Teng, J. G., Yu, T., Wong, Y. L., and Dong, S. L. (2007). "Hybrid FRP concrete-steel tubular columns: Concept and behavior." Constr. Build. Mater., 21(4), 846–854.
[19] Han, L. H., Tao, Z., Liao, F. Y., & Xu, Y. (2010). Tests on cyclic performance of FRP–concrete–steel double-skin tubular columns. Thin-Walled Structures, 48(6), 430-439.
[20] Yu, T., Wong, Y. L., Teng, J. G., Dong, S. L., & Lam, E. S. (2006). Flexural behavior of hybrid FRP-concrete-steel double-skin tubular members. Journal of Composites for Construction, 10(5), 443-452.
[21] Abdelkarim, O. I., ElGawady, M. A., Gheni, A., Anumolu, S., and Abdulazeez, M. (2016). "Seismic Performance of Innovative Hollow-Core FRP–Concrete–Steel Bridge Columns." J. Bridge Eng., 10.1061/(ASCE)BE.1943-5592.0000985 , 04016120.
[22] Abdelkarim, O. I. and ElGawady, M. A. (2014). "Analytical and Finite-Element Modeling of FRP-Concrete-Steel Double-Skin Tubular Columns." J. Bridge Eng., 10.1061/(ASCE)BE.1943-5592.0000700 , B4014005.
[23] Ozbakkaloglu, T. and Idris, Y. (2014). "Seismic Behavior of FRP-High-Strength Concrete-Steel Double-Skin Tubular Columns." J. Struct. Eng., 140(6), 04014019.
[24] Zhang, B., Teng, J. G. and Yu, T. (2012). "Behaviour of hybrid double-skin tubular columns subjected to combined axial compression and cyclic lateral loading." Sixth International Conference on FRP Composites in Civil Engineering (pp. 1-7). Rome, Italy.
[25] Abdelkarim, O. I. and ElGawady, M. A. (2016a). "Performance of hollow-core FRP–concrete–steel bridge columns subjected to vehicle collision." Engineering Structures, 123, 517-531.
[26] He, R., Grelle, S., Sneed, L. H., and Belarbi, A. (2013). "Rapid repair of a severely damaged RC column having fractured bars using externally bonded CFRP." Compos. Struct., 101, 225–242.
[27] Saini, A., and Saiidi, M. S. (2013). "Post-earthquake damage repair of various reinforced concrete bridge components." Caltrans Final Rep. CA 142179, Caltrans, Sacramento, CA.
[28] Fakharifar, M., Chen, G., Wu, C., Shamsabadi, A., ElGawady, M., and Dalvand, A. (2016). "Rapid repair of earthquake-damaged RC columns with prestressed steel jackets." J. Bridge Eng., 10.1061/(ASCE)BE .1943-5592.0000840, 04015075.
[29] ACI Committee 318 (2014). "Building Code Requirements for Structural Concrete (ACI318-14) and Commentary (318R-14)." American Concrete Institute, Farmington Hills, Mich., pp. 509.
[30] ASTM A1067 / A1067M-12a, Standard Specification for Test Coupons for Steel Castings, ASTM International, West Conshohocken, PA, 2012.
[31] FiberGlass systems. (2013). "Green Thread HP 16 Product Data." National Oilwell Varco, San Antonio, TX.
[32] FiberGlass systems. (2012). "F-Chem Product Data." National Oilwell Varco, San Antonio, TX.
[33] ASTM D3039 / D3039M-14, Standard Test Method for Tensile Properties of Polymer Matrix Composite Materials, ASTM International, West Conshohocken, PA, 2014.
[34] Fyfe Co. LLC. (2002). "Tyfo SHE-51 composite." Fyfe Co. LLC., San Diego.
[35] Calvi, G. M., & Task Group Seismic Design and Assessment Procedures for Bridges International Federation for Structural Concrete. (2007). Seismic bridge design and retrofit: structural solutions; state-of-art report. Internat. Federation for Structural Concrete.
[36] Federal Emergency Management Agency (FEMA 461). (2007). "Interim Testing Protocols for Determining the Seismic Performance Characteristics of Structural and Nonstructural Components." Federal Emergency Management Agency, Washington, USA.
[37] Idris, Y. and Ozbakkaloglu, T. (2016). "Behavior of square fiber reinforced polymer–high-strength concrete–steel double-skin tubular columns under combined axial compression and reversed-cyclic lateral loading." Engineering Structures, 118, 307-319.